Unveiling the Mechanical and Microstructural Properties of SiC Reinforced Aluminum Wires recycled from scraps by Friction Stir Extrusion.

Muhammad Adnan[a], Gianluca Buffa[a*], Amir Baghdadchi [b], Vivek Patel[b], Livan Fratini[a]

[a]Department of Engineering, University of Palermo, Viale delle Scienze, 90128 Palermo, Italy

[b]Department of Engineering Science, University West, Trollhättan 46186, Sweden

**Corresponding* author. tel.: +39-09123861869. *E-mail address:* gianluca.buffa@unipa.it

Abstract

Friction Stir Extrusion (FSE) has been proven as an effective solid-state process to directly recycle metal chips into high-quality wires/rods/tubes. However, the demand for Al-based composite wires with enhanced properties is substantial, and achieving a uniform distribution of the strengthening phase within the composite wire by establishing a robust metal/ceramic interface remains a significant challenge. In this study, AA6082 Aluminum alloy wires reinforced with 12.5 vol.% SiC particles, exhibiting homogeneous particle distribution and superior mechanical properties, were successfully produced through the FSE technique. The investigation focused on examining the influence of processing parameters and the addition of SiC reinforcement on the microstructure and mechanical characteristics of the extruded wires. Scanning electron microscopy (SEM), Electron Backscatter Diffraction (EBSD), together with microhardness, bending, and tensile tests, were used to comprehensively analyze the resulting properties. The findings demonstrate a substantial enhancement in the wires mechanical properties due to the SiC particles. Both tool rotation and tool force were varied during the experimental campaign. Notably, the reduction in porosity and grain refinement resulted in a 12.78% increase in tensile strength and an 18.6% improvement in microhardness compared to Al 6082 alloy extruded wires. Grain orientation analysis revealed a fully recrystallized microstructure with a weak texture. Furthermore, the study evaluated power consumption and surface roughness while assessing the feasibility of deposition, thereby highlighting the potential application of this technique in advanced additive manufacturing processes.

Keywords: Friction stir extrusion, aluminum alloys, silicon carbide, microstructure

Graphical abstract

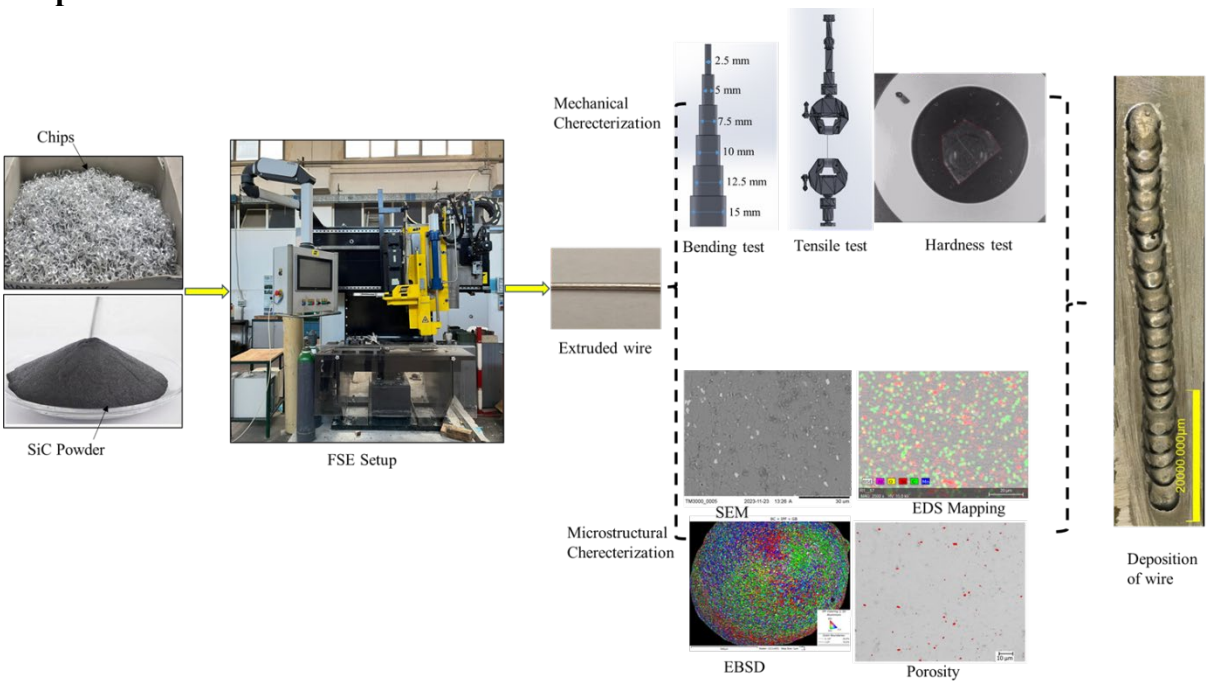

1. Introduction.

Due to its remarkable properties, including high strength-to-weight ratio, ductility, and durability, aluminum and its alloys are highly desirable for various industries. This has led to a significant increase in global aluminum demand over the last years [1]. Substituting aluminum for heavier steel in designs can result in substantial fuel savings, with studies suggesting potential savings of 5-7% for every 10% weight reduction [2].

Aluminum production is highly energy-intensive, relying on electrolytic reduction processes that require large electric currents [3]. Energy consumption accounts for 20% to 40% of production costs [4]. Consequently, recycling processes offer a more environmentally sustainable alternative, utilizing scrap aluminum alloys as the basis for producing aluminum metal matrix composites. Studies indicate that recycling aluminum can potentially mitigate over 94% of the environmental impact related to global warming and fossil fuel depletion due to primary aluminum production processes [3]. Furthermore, economic advantages arise from the reduced costs associated with utilizing scrap materials.

Conventional aluminum recycling methods, such as remelting and recasting, are energy-intensive and result in significant material loss due to oxide formation during melting [5]. To overcome these challenges, solid-state recycling (SSR) techniques have been developed, which process alloy scraps through plastic deformation below the solidus temperature [6]. This approach significantly reduces energy consumption to just 5% of that required by conventional methods, which involve remelting scraps. Additionally, SSR uses up to 95% of the starting material, avoiding the typical 20% metal loss caused by oxidation, burning, and slag contamination. [7]. Various techniques fall under solid-state recycling, including Equal Channel Angular Pressing (ECAP) [8], Shear Assisted Processing and Extrusion (ShAPE) [9], hot extrusion and hot rolling method [10], consolidation [11], forging [9], and sintering [13]. FSE is a promising solid-state recycling method, similar to Friction Stir Welding (FSW), where frictional heat softens materials for extrusion. Recent advancements have made FSE a preferred method for directly converting

metal powders, chips, or billets into high-quality wires or rods. [7]. While FSE can be applied to various light metal alloys, the majority of research focuses on aluminum, magnesium, or their composites due to industrial demand and feasibility.

Aluminum-based composites incorporating ceramic reinforcing particles exhibit remarkable properties including high strength-to-weight ratio, enhanced elastic modulus, rigidity, and exceptional wear resistance [14,15]. These materials find extensive applications across diverse industries such as aerospace and automobile manufacturing [16,17]. Al_2O_3 [18] B_4C [5], SiC [6] TiC, and TiB_2 [19] are common reinforcement ceramic particles for aluminum matrix composites. Among these, SiC holds a prominent position due to its unique properties [20]. Research findings have consistently demonstrated that the incorporation of SiC significantly enhances various mechanical properties of composites, including Young's modulus, UTS, fatigue resistance, hardness, and wear resistance. This attribute makes SiC widely sought after in the construction and machinery sectors [21]. In Al 6082/SiC composites, aluminum serves as the matrix material while SiC particles act as the reinforcement phase. This synergistic combination harnesses the advantageous properties of both materials, such as low density, ease of production, and high specific stiffness, leading to superior performance characteristics in the resulting composite material [22]. A few studies have sought to enhance composite properties through various methodologies, including heat treatment and the incorporation of hardening phases [23]. Gronostajski et al. [24] proposed a method for fabricating composites using Al, $AlCu_4$ alloy, and $AlMg_2$ alloy granulated chips with varying amounts of tungsten powder addition. Their work emphasized that the addition of tungsten led to reduced porosity, improved diffusion bonds, and relative density exceeding 98%. However, they observed that heat treatment resulted in an increase in tensile strength but a decrease in ductility. Fogagnolo et al. [25] investigated the introduction of Al_2O_3 into aluminum alloy 6082 chips by cold pressing and hot extrusion and compared the properties with the original one. The author highlighted that the ultimate tensile strength (UTS) and the hardness increased than original alloy. Samuel [26] explored the direct conversion of granulated aluminum Al-2014 scrap alloy with Al_2O_3 Saffil fiber into final products via hot extrusion process, revealing that the addition of 10 vol% of Al_2O_3 Saffil fiber YS, UTS, and strength of the composite have been increased than Al-2014 conventional alloy. Tekkaya et al. [6] proposed the addition of SiC particles to aluminum alloy 6060 but encountered challenges due to particle dispersion. This led to damaged extruded profiles and a rough surface, resulting in decreased strength as indicated by tensile tests. Razzaq et al. [27] fabricated composites by adding fly ash to aluminum alloy 6063, observing that increasing fly ash content led to increased microhardness and porosity but decreased bulk density and Charpy impact energy. Baffari et al. [28] demonstrated the feasibility of producing Al-SiC metal matrix composite wire through FSE of aluminum chips and examined the microstructure of composite wires. Alimi et al. [5] investigated aluminum AA6061 chips reinforced with B4C- and ZrO_2-based ceramic particles via hot extrusion, finding that compressive strength and hardness increased with up to 5% additional particles before declining due to material agglomeration. Recently, Li et al. [29] investigated the effect of TiB_2 on the fabrication of AA7075/TiB_2 composites using friction consolidation techniques. Their findings revealed that the addition of 24 vol% TiB_2 significantly enhanced the tensile strength and wear resistance of the composite. Sherafat et al. [30] explored the incorporation of powdered aluminum into 7075 aluminum chips during direct conversion, discussing the impact of powder content and extrusion temperature on composite mechanical properties. They noted that increasing chip percentage improved strength but reduced ductility.

Based on the literature review, it is evident that existing studies predominantly focus on composite production through methods such as hot extrusion or ECAP, wherein reinforced particles are added. While effective for recycling aluminum alloy, these techniques necessitate higher heat inputs. In contrast, FSE offers a low-heat alternative for material plasticization and extrusion. However, research on producing composite wires via FSE remains limited, with most studies producing wires exceeding 2.5 mm in diameter. Such wires have limited industrial applicability, particularly in contexts requiring thinner composite wires. Thin composite wires hold significant potential for diverse applications such as composite-cored conductors, electrical applications, and fillers in arc welding and arc welding-based additive manufacturing processes.

This study explores the recycling of aluminum alloy AA6082 chips, reinforced with SiC particles, through FSE to manufacture AA6082/SiC thin composite wires with a diameter of 1.6 mm. The research aims to investigate the impact of process parameters on the mechanical and microstructural properties of the AA6082/SiC composite. Additionally, it compares the properties of the composite wire with those of AA6082 chips extruded wire. The study also assesses the power consumption and surface roughness of the extruded wire. Finally, at optimal process parameters, the extruded composite wire was employed as a filler rod in the WAAM process to demonstrate the applicability and potential of the process in a "closed loop" production process involving FSE, WAAM and machining.

2. Materials and Methods

2.1. Material

Aluminum chips were prepared by CNC machining from a bulk rod of AA6082-T6. These chips were crafted to dimensions measuring between 3.40-3.80 mm in length, about 1.60 mm in width, and 0.09 mm in thickness, resulting in a surface area of approximately 12.34 mm² per chip. To eliminate any potential surface contamination or remnants of machining oil, the chips underwent a cleaning process adhering to the ASTM G131-96 standard, utilizing acetone for degreasing purposes. Subsequently, post-cleaning and drying, the chips were meticulously mixed with SiC powder to ensure uniform dispersion. The average SiC particle size was 3µm. Detailed chemical composition and physical properties of the AA6082 chips are outlined in table 1 and table 2 respectively.

Table 1. Chemical composition % w/w of the used AA6082 [31].

Chemical composition % w/w								
Al	**Cr**	**Cu**	**Fe**	**Mg**	**Mn**	**Si**	**Ti**	**Zn**
95.2-98.3	≤0.25	≤0.1	≤0.5	0.6-1.2	0.4-1.0	0.7-1.3	≤0.1	≤0.2

Table 2. Mechanical Properties of AA6082 in O, T4, and T6 state [31].

Heat treatment	UTS (MPa)	Elongation (%)	Hv
O	130	27	35
T4	200	14	65
T6	290	10	95

2.2. Experimental Activity

The experimental campaign for FSE was conducted using the FSW machine ESAB LEGIO, aiming to produce Al 6082/SiC wires by incorporating SiC powder into Aluminum alloy Al6082 chips and comparing them with Al 6082 alloy wires (Fig. 1). Some of the authors [31] focused on optimizing the tool design to improve the extrusion rate. Tool diameter of 14.7 mm, tool shoulder angle of 10 degrees, and extrusion hole diameter of 1.6 mm, were kept constant for all experiments based on the results of a preliminary campaign. The experimental plan, outlined in Table 3, involved varying tool force (15, 18, and 21 kN) and rotational speed (400, 500, and 600 RPM). Various SiC powder percentages (10%, 12.5%, and 15%) were evaluated at a preliminary stage, with a noticeable decrease in extrusion rate with increasing SiC content. For this research, a 12.5% SiC powder concentration was selected for all the experiments. Each test configuration was repeated three times to ensure reliability and consistency in the results.

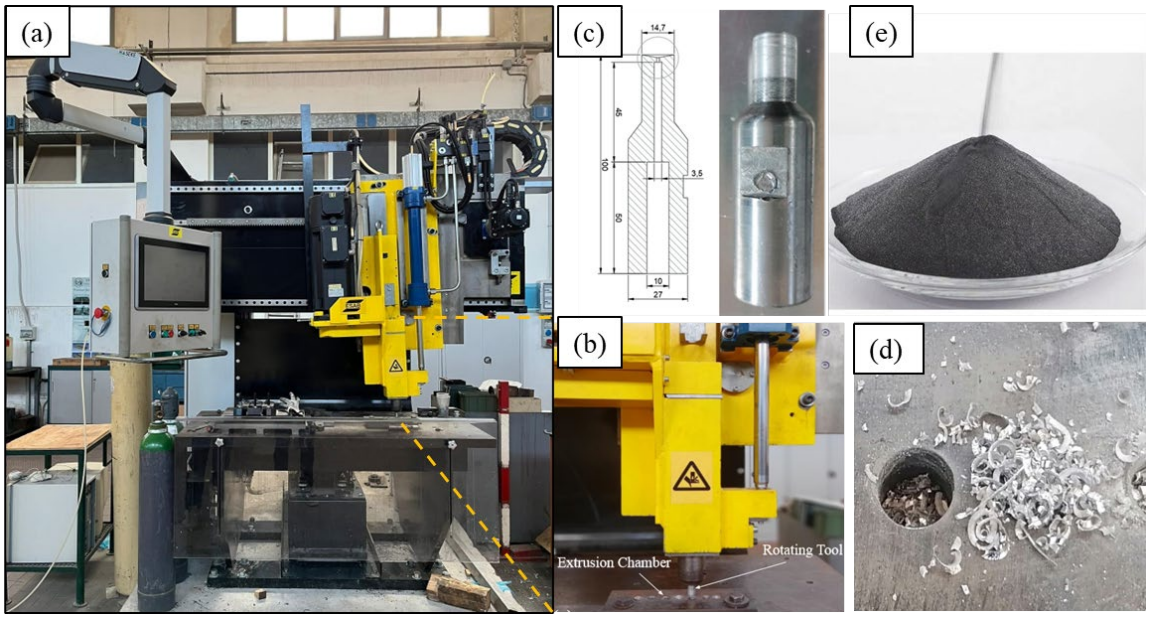

Figure. 1 (a) FSE setup for the experimental campaign (b) FSE Fixture (c) Extrusion tool (d) Extrusion Chamber (e) SiC powder.

Table 3. Experimental conditions for FSE.

Sample label	Tool Rotation [RPM]	Force [kN]
S400-15	400	15
S400-18	400	18
S400-21	400	21
S500-15	500	15
S500-18	500	18
S500-21	500	21
S600-15	600	15
S600-18	600	18
S600-21	600	21

The average length of the produced wires was approximately 600 mm. Subsequently, specimens were extracted from each extrudate to evaluate material properties through mechanical and

microstructural analyses. Tensile tests were carried out in accordance with ASTM D2256 standards. For each test, a 250 mm wire was mounted in a tensile testing machine (Figure 5b), which applied a constant rate of extension until the sample fractured. The breaking force was recorded for each test. Three tests were conducted for each sample to ensure the consistency and reliability of the results. Cross-sections of the wires were prepared by mounting, polishing, and etching with Weck's reagent (100 mL H2O, 1g NaOH, 4g KMnO4) for 15 seconds to reveal microstructural features. Vickers microhardness testing was then performed along the diameters of the cross-sectioned samples. Furthermore, bending tests were conducted to assess the ductility of the produced wires, utilizing various bending radii including 15, 12.5, 10, 7.5, and 5 mm. These tests aimed to determine the feasibility of wrapping the obtained wire around a reel. For microstructural analysis, SEM (ZEISS SUPPEA5) equipped with EDS was employed to examine the presence and dispersion of SiC particles. The SEM was equipped with EBSD detector for grain refinement analysis. During EBSD analysis, the acceleration voltage was set to 20 kV, the sample tilt angle to 70°, and the working distance to 9 mm. Step size for the entire cross section and high magnified regions were 1 μm and 0.3 μm, respectively. The Aztec Crystal 1.1 software from Oxford Instruments was used to analyze the EBSD results. Porosity measurement was conducted using an automated optical microscope. Surface roughness was assessed by using surface roughness tester and 3D profiles have been created by using Profilm. Finally, a commercially available Fluke 435 power quality analyzer, capable of recording voltage, current, and power history, was used to perform the power consumption analysis.

3. Results and discussion

3.1 Macroscopical Observation

First, a visual inspection was carried out on the produced wires. Fig. 3 illustrates the macroscopical observations of the extruded Al 6082/SiC wires surface under various process parameters, as detailed in Table 2. The rotational motion of the tool facilitates material mixing and stirring within the extrusion chamber. Concurrently, the movement of the extrusion tool along the z-axis results in the plasticized material being extruded into the central hole of the inserted tool. Notably, specimens produced at lower rotational speeds and forces exhibited twisting and cold tearing. Insufficient heat generation at low rotational speeds, such as 400 rpm, was identified as a contributing factor to increased extrusion defects. Conversely, wires produced at high force and rotational speeds (500 and 600 rpm) displayed smooth surfaces devoid of cracks along their entire length. Particularly, wires extruded at 600 rpm exhibited superior surface quality, attributed to enhanced heat generation at higher rotational speeds. Proper choice of process parameters has a strong effect on Al 6082/SiC extruded wires. At low RPM, the dispersion of SiC is low and the produced heat is not enough to bond aluminum with SiC, resulting in agglomeration of reinforced particles, brittleness, and surface roughness of the extruded wire, as it will be better explained in the following. By increasing the tool force, the extrusion rate also increases (please refer to the power consumption paragraph 3.5), preventing overheating in the matrix.

It is important to note that during the preliminary experiments, a further increase in tool rotational speed led to the formation of hot cracks and increased surface roughness. In fact, an increase in tool rotation generates higher frictional heat, which can exceed the materials tolerance, leading to localized thermal stresses and the formation of hot cracks. In particular, higher temperatures are reached at the interface between the extruded wire and the extrusion

channel due to the additional friction. In this way, for high tool rotation values, local micro-fusions can occur. Together with the elevated stress at the edge of the die, the latter phenomenon can result in an initial crack on the outer surface of the wire which can propagate toward its inner part [31,32]. The presence of SiC can magnify the hot crack phenomenon due to the increased friction at the contact interface between the material and the extrusion channel, as it will be better explained in the following.

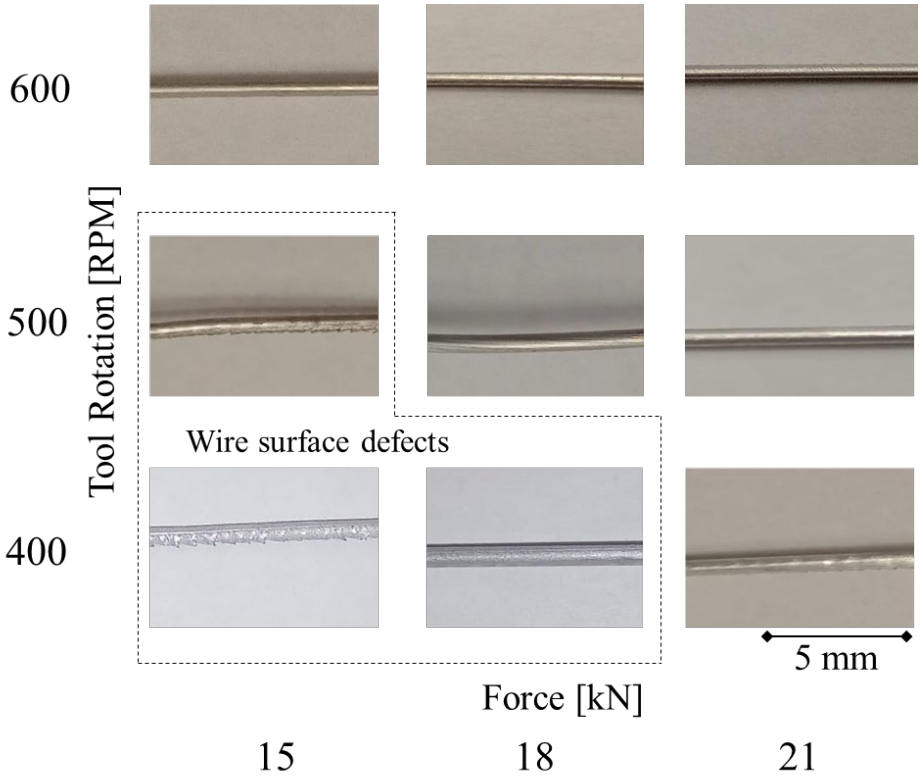

Figure 3. Extruded Al 6082 /SiC wires surface at various process parameters.

The cross-sectional and longitudinal surfaces of the samples were examined using an optical microscope in order to identify possible defects as well as the flow of the SiC particles. Fig. 4 shows the results obtained for the case study S600-18 with and without the SiC powder. The flow and dispersion of SiC appear uniform across cross-sectional of the sample, as compared to the same process conditions without the SiC. No discernible defects, such as voids, are apparent in the wires.

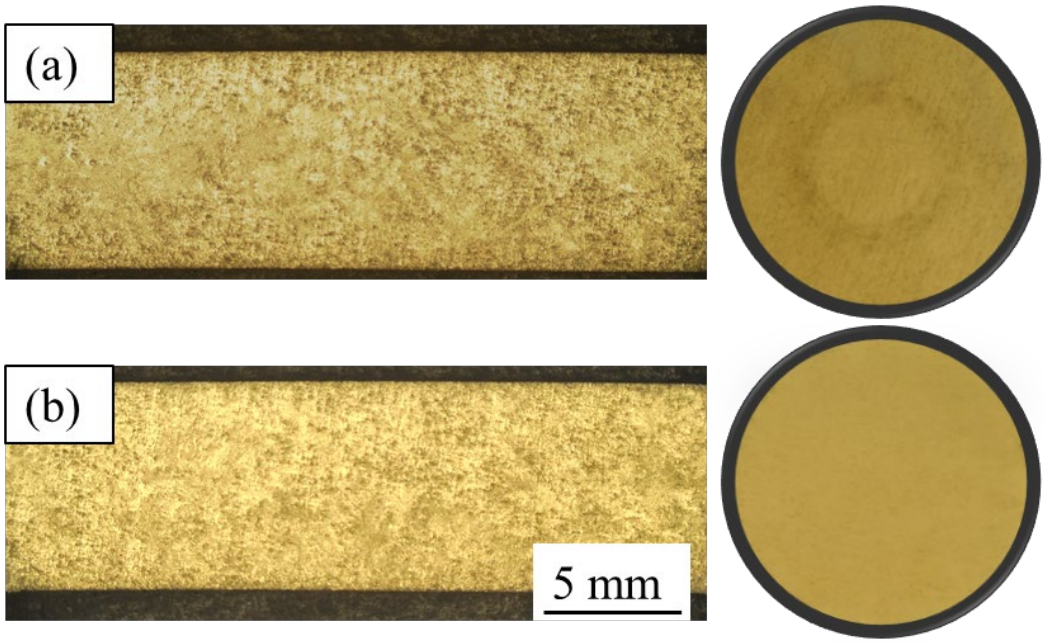

Figure 4. Longitudinal and crossectional view of (a) Al 6082/SiC composite wire (b) Al 6082 wire – S600-18 case study.

3.2. Mechanical characterization

Tensile tests were conducted on the wires according to ASTM D2256 standards. Fig. 5a illustrates the results compared to the ones of the wires produced with no powder, while Fig. 5b showcases the experimental fixture utilized for the tests. The analysis of the processed samples without SiC particles reinforcement revealed a well-defined trend of the ultimate tensile strength (UTS) as a function of tool force and rotation. Specifically, the UTS increases with both increasing tool force and rotation speed. It is noted that minimum UTS was obtained for the case study S400-15, i.e. the one corresponding to the minimum heat input among the ones considered in this study, for which the maximum UTS recorded was approximately 54 MPa. As for the other case studies within the surface defect window, UTS increases to a maximum of about 160 MPa (S400-18). However, at tool force values of 18 kN and 21 kN, significantly higher resistance was observed. The maximum value of average tensile strength for non-reinforced extruded wires was obtained with an extrusion force of 21 kN, for which average UTS ranged between 190 and 196 MPa. It is observed that at 21 kN, the UTS of all three samples is similar to the UTS of sample S600-18. In other words, the increasing trend observed moving from low tool rotation and tool force values towards higher values seems to reach a plateau. This can be attributed to the competition between two factors: higher force leads to both an increase in the extrusion rate, resulting in lower processing temperature, and in an increase of the friction forces work, increasing temperature. In this way, similar material flow conditions are reached. By incorporating 12.5% reinforcement SiC particles, a similar UTS trend was obtained against variations of both tool force and rotation. However, the overall strength of each sample has been increased with the addition of SiC particles. This enhancement can be elucidated through several factors. Foremost, the phenomenon of load transfer from the pliant matrix to the rigid reinforcement particles during tensile testing must be considered. This load transfer, facilitated by the uniform dispersion of SiC particles within the aluminum matrix and the establishment of robust interfacial bonding, engenders an enhancement in tensile

strength. By comparing the UTS properties at optimal process parameters, i.e. S600-18, it arises that UTS of Al6082/SiC and Al6082 wire is 214 MPa and 190 MPa, respectively, with a 12.78% increment.

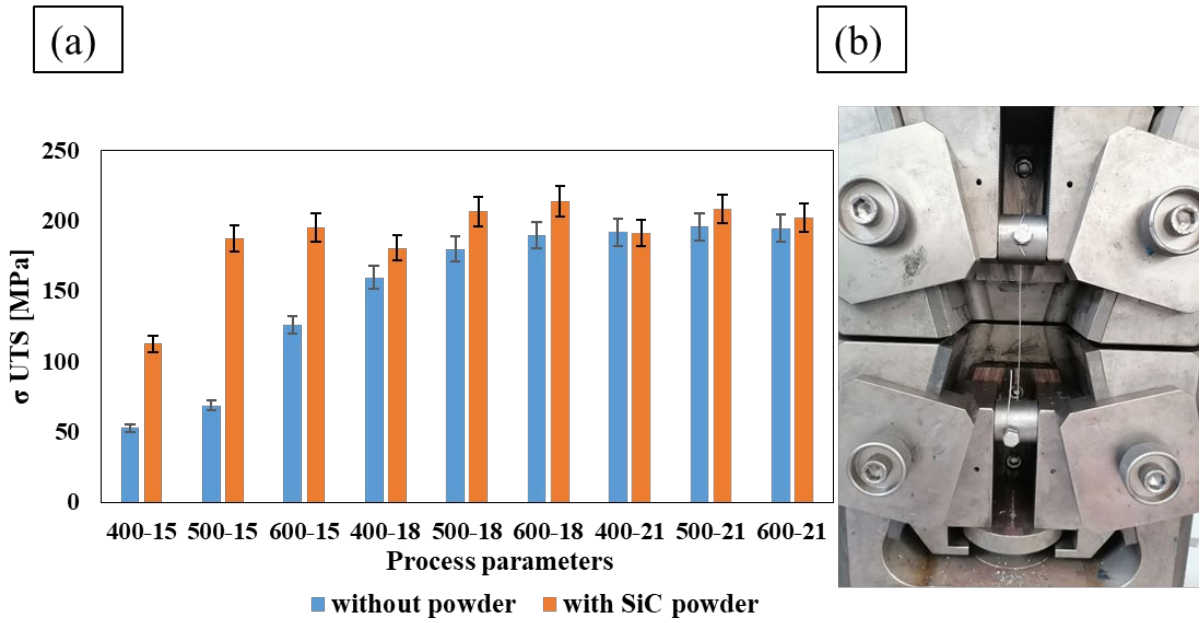

Figure 5 (a) Tensile test Results (b) Experimental Fixture for Tensile testing of wire.

Bending tests were conducted utilizing the experimental setup depicted in Fig. 6a. Extruded wires were wrapped around the fixture, characterized by different radii, in order to assess the bendability of the wire. It is worth noticing that this is an important test for the industrial application of recycled wires, which can be effectively used as filler wires in arc welding or arc welding-based additive manufacturing. Observations revealed that the minimum bending radius could be achieved with an extrusion force of 18 and 21 kN, regardless of the tool rotation rate. Conversely, with an extrusion force of 15 kN, a notable reduction in wire ductility was observed. For sample S400-15, inadequate bonding between chips led to fracture with the largest radius (Fig. 6b). Although increasing the tool rotation rate enhanced ductility, sample S600-15 experienced hot cracking, limiting its ductility and resulting in bending failure with a radius of 10 mm. As for Al 6082/SiC composite wires, it was noted that at low RPM and force, the wires bendability was minimal. This was attributed to poor bonding between chips and reinforced particles, exacerbated by the agglomeration of SiC particles due to low RPM. Consequently, the bendability of the Al 6082/SiC composite wire was lower than that of the unreinforced wire under these conditions. However, with increasing process parameters, the bendability of the reinforced wire increased significantly. At S600-18, the bending behavior of the reinforced wire resembled that of the unreinforced wire. This improvement can be attributed to the uniform dispersion of reinforced particles and the establishment of proper bonding between chips, resulting in a notable enhancement in properties. Table 4 reports the bendability of the processing window at various radii.

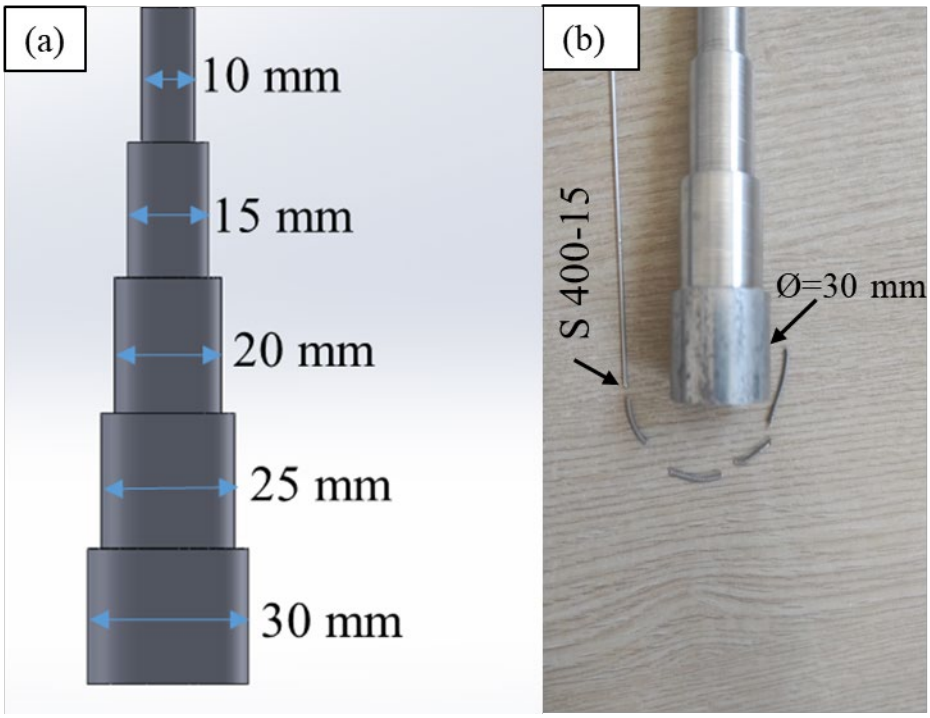

Figure 6. Bendability of wire (a) Bending tool stages (b) sample S400-15.

Table 4 . Bendalbity of extruded samples at various bending radii.

	Bending Radii (mm)									
	15		12.5		10		7.5		5	
Process Parameters	Al 6082	Al 6082 /SiC	Al 6082	Al 6082/SiC	Al 6082	Al 6082/SiC	Al 6082	Al 6082/SiC	Al 6082	Al 6082/SiC
S600-21	✓	✓	✓	✓	✓	✓	✓	✓	✓	✓
S500-21	✓	✓	✓	✓	✓	✓	✓	✓	✓	✓
S400-21	✓	✓	✓	✓	✓	✓	✓	✓	✓	✓
S600-18	✓	✓	✓	✓	✓	✓	✓	✓	✓	✓
S500-18	✓	✓	✓	✓	✓	✓	✓	✓	✓	✓
S400-18	✓	✓	✓	✓	✓	✓	✓	✗	✗	✗
S600-15	✓	✓	✓	✓	✓	✓	✗	✗	—	—
S500-15	✓	✗	✗	✗	✗	✗	—	—	—	—
S400-15	✗	✗	—	—	—	—	—	—	—	—

The microhardness assessment involved three equally spaced indentations made across the cross-section of each extruded wire, extending from the center to the boundary. The average hardness values were plotted, as depicted in Fig. 7. In particular, Fig. 7a presents the microhardness comparison between specimens from the experimental trials, illustrating both the reinforced Al 6082/SiC wires and the unreinforced Al 6082 wires. A sketch showing the indentation loci is provided in Fig. 7b. The analysis of the microhardness values from the unreinforced samples reveals an increase in hardness with increasing heat input, i.e. an increase in rotational speed and force. For the unreinforced sample S400-15 the average microhardness

was 71 HV, which increases to 96 HV for the sample S600-21. Moreover, it was noted that, for all the considered case studies, the hardness value slightly increases from the center to the edge of the measured sample. This increase can be attributed to the formation of recrystallized fine grains and the reduction in grain size from the center to the edge during the FSE process, as will be better discussed in the following. In fact, it is well-established that materials with finer grains exhibit increased hardness and strength due to grain boundaries restricting dislocation motion. As for the hardness of samples containing 12.5% SiC reinforcing particles, a substantial increase in microhardness is observed for all the case studies. For the sample S600-18 the hardness increased from 90 to 106.8 HV by the addition of SiC, which is 18.6 % increment based on unreinforced Al 6082 wire and 205% higher with respect to the AA6082-O base material (avg 35 HV). This enhancement can be attributed to the reinforcing particles acting as barriers against dislocation movement, thereby increasing dislocation density, a primary factor contributing to hardness elevation. It is worth noting that the reported hardness values represent the average measurements taken at three points along the cross-section of the wire: the center, middle, and edge. For the unreinforced aluminum alloy wire, the hardness values for samples S400-18 (HV 71) and S400-21(HV 70) were lower (or comparable) to those of S400-15 (HV 71). However, increasing UTS was obtained with increasing tool force for the above process conditions. This can be explained by observing the presence of internal defects, i.e. porosities, as it will be better analyzed in the following.

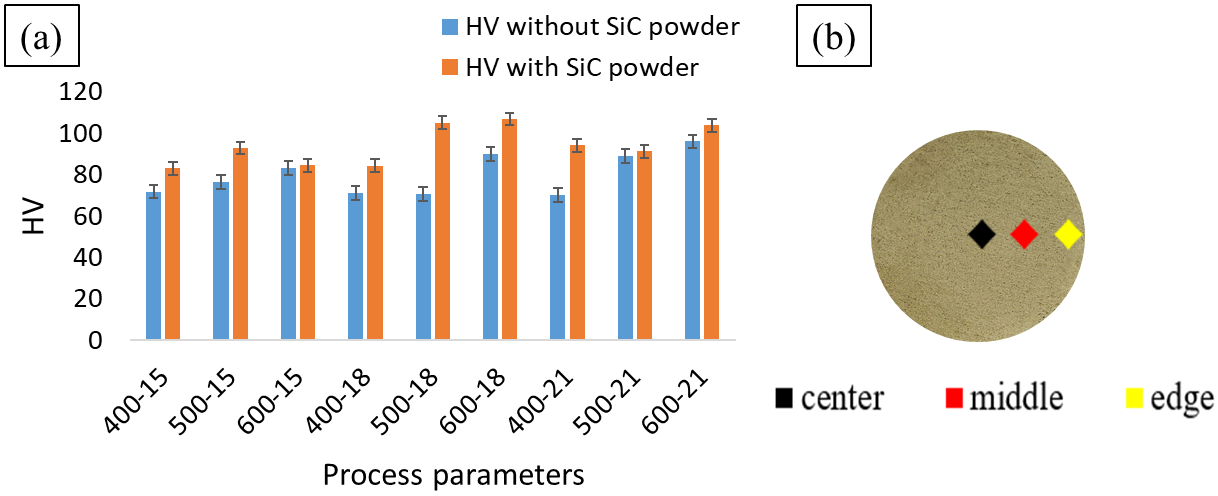

Figure 7. (a) Average hardness value for each case study (b) sketch of the indentation loci.

3.2. Microstructural characterization

Fig. 8 illustrates the SEM acquisition on the cross-section of sample S400-15. At low heat input, i.e. low tool force and rotation, the agglomeration of SiC has been observed (Fig. 8a). The particle distribution within the matrix strongly depends on the different process parameters considered: at the lowest rotational speed, the distribution appears non-uniform, which leads to the brittleness of the wire and reduced tensile properties previously observed. Fig. 8b illustrates the agglomeration of SiC particles at higher magnifications and their corresponding EDS

mapping (Fig. 8c-j). The SEM image of the cross-section of Al 6082/SiC wire is shown in Fig. 9 for the S600-18 case study. The specimen exhibits a nearly uniform SiC particle distribution, and a good bonding between aluminum matrix and SiC particles has been observed, which causes improvement of properties and reduced porosity. EDS mapping and analysis (Fig 9b-f) confirms the uniform dispersion of SiC particles in the entire cross-section of wire, which results in an improvement in mechanical and microstructural properties.

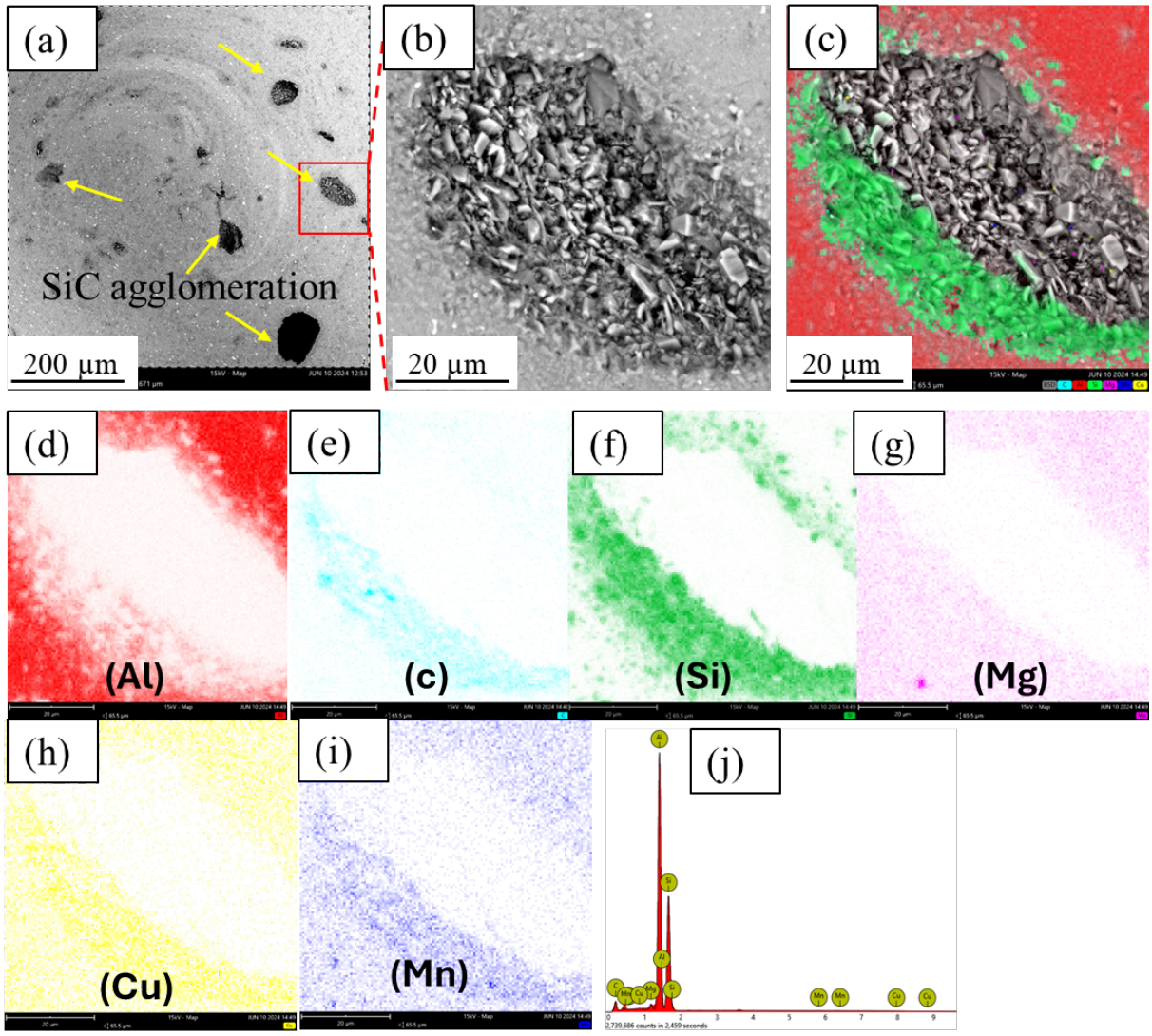

Figure 8. (a) SEM image of the cross-section of Al 6082/SiC wire, sample S400-15 (b) SEM image at higher magnification, and (c-J) EDS mapping of the corresponding cross-section representing the agglomeration of SiC particles.

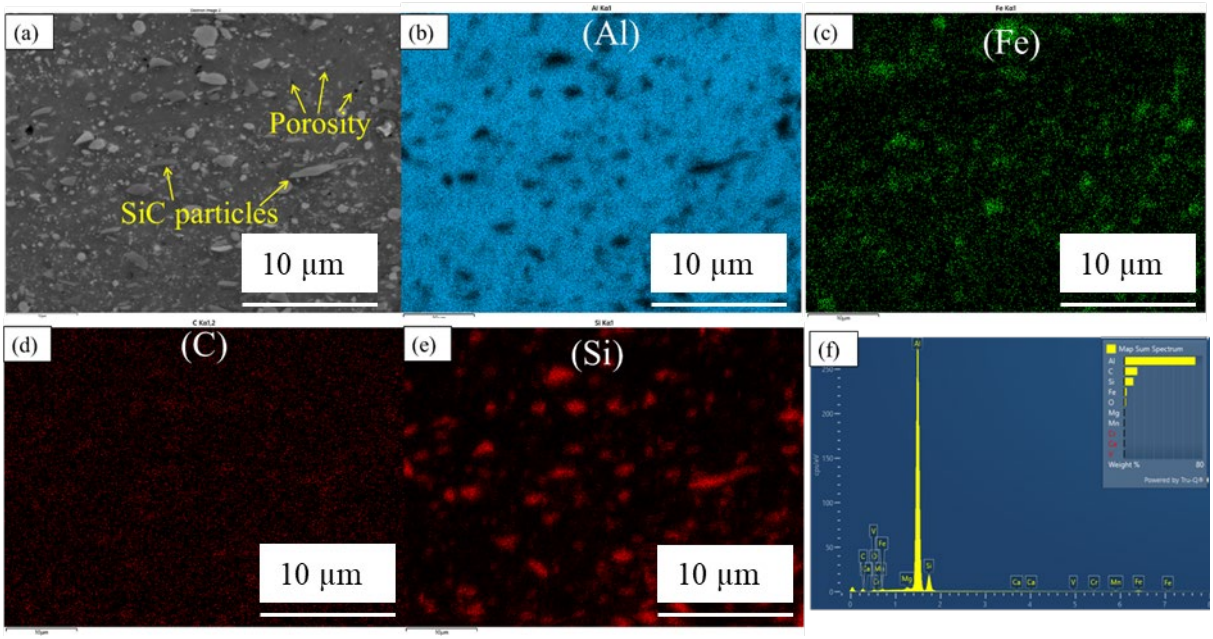

Figure 9. (a) SEM image of the cross-section of Al 6082/SiC wire, sampleS600-18 (b-f) EDS mapping of the corresponding cross-section representing the uniform dispersion of SiC particles.

EBSD was employed to conduct a comparative analysis on Al 6082 and Al 6082/SiC composite wires for the S600-18 case study, with the aim was to investigate the effect of SiC on the grain size and orientation. The EBSD inverse pole figure (IPF) maps of FSE extruded Al6082 alloy wire of sample S600-18 are shown in Fig. 10. The entire cross section (Fig 10a) and longitudinal section (Fig. 10b) have been considered representing a FCC structure having a large number of dislocations climb and cross-slip. Moreover, the grains at the center of the cross-section are comparatively larger in size than the ones at the edges, due to higher shear deformation. In fact, during the extrusion process, the edges of the tool act as a hindrance to the growth of grains near to its contacting surface causing small size grain formation. In the longitudinal section, grains are oriented toward the extrusion directions. Fig. 11 exhibits the comparative analysis of the IPF maps of extruded Al 6082 and Al 6082/SiC composite wire cross-section at higher magnification, for sample S600-18. It is noted that the grains are more equiaxed with uniform sizes in Al 6082/SiC composite wire (Fig. 11(b)) compared to aluminum wire (Fig. 11a). The average grain size decreases from 7.6±0.3 µm to 5.6±0.3 µm when moving from the Al 6082wire to the Al 6082/SiC composite wire. This reduction in grain size is due to the reinforced SiC particles. During the extrusion process, SiC particles can serve as heterogeneous nucleation sites, significantly enhancing the crystal nucleation rate of the aluminum matrix. This results in notable grain refinement [33]. It is worth noticing that grain size is different in different regions. As mentioned above, the grain size decreases from the center to the edge of the wire in Al 6082 and Al 6082/SiC composite wire.

In order to observe the grain morphology in the longitudinal section of the wire, two points of analysis were identified at the center and at the edge of the wire (Fig. 12). In particular, Fig. 12a and 12b present IPF map of the Al 6082 wire longitudinal section at the center and at the edge, respectively. This region comprises fine-recrystallized grains with strong crystallographic orientations 〈001. The grain size slightly increases in the center while decreasing at the edge and elongates toward the extrusion direction, indicating alteration of strain condition. It is also

seen that at the edge the thickness of some elongated grains decreases due to the geometrical requirement of strain. Fig. 12c and 12d represent the same maps for the Al 6082/SiC composite wire. It is seen that with the addition of SiC powder, the grains are more uniformly distributed in the longitudinal sections. formation of LAGBs inside the large grain interior is clearly observed due to dislocation accumulation induced by the shear strain. Continuous absorption of the dislocations in the grain boundaries leads to an increase in the misorientation angle. Some of the LAGBs transform into HAGBs when the grain misorientation exceeds 15◦ dividing the large grains into smaller grains. It is also seen that the thickness of some elongated grains decreases due to the geometrical requirement of strain. An increase in the strain induces progressive lattice rotation and grain subdivision, which transforms the thin elongated grains into new fine-recrystallized grains.

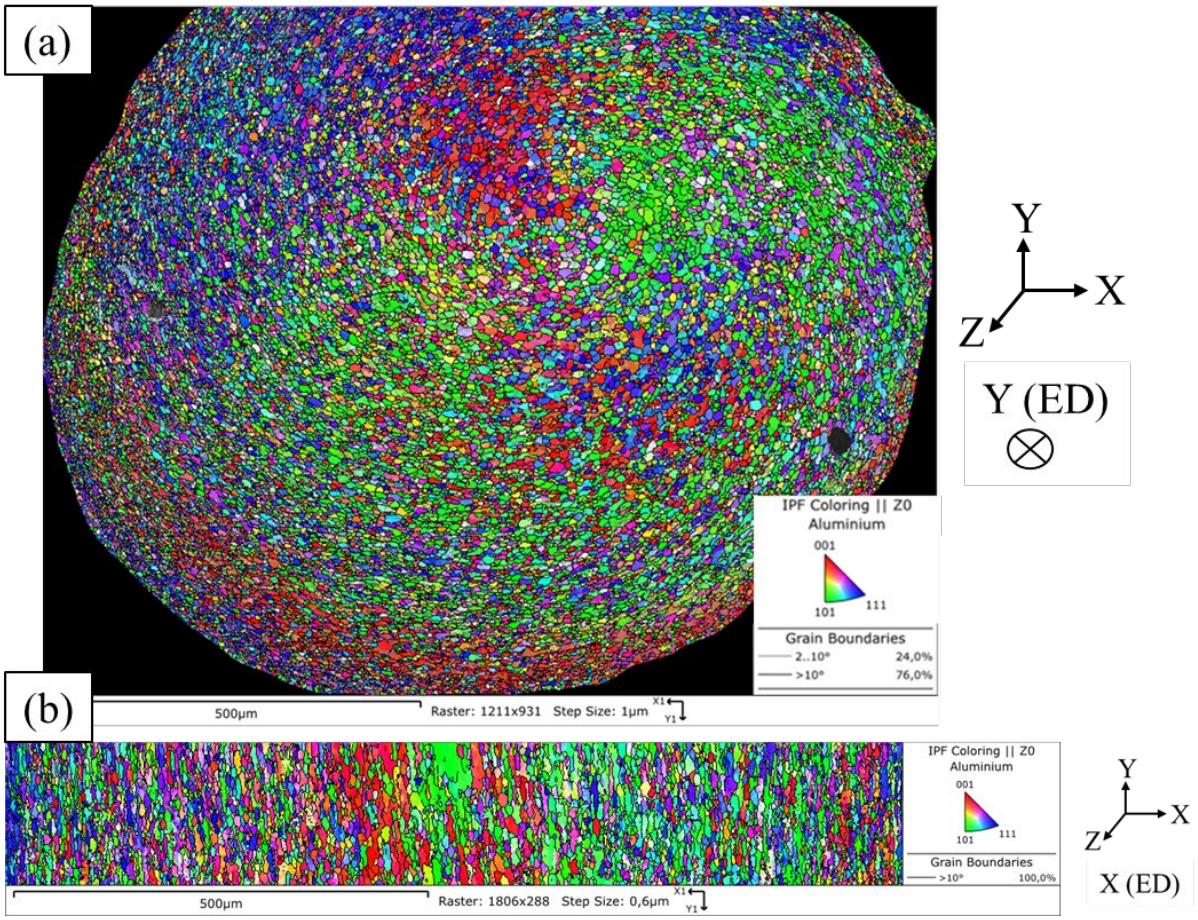

Figure 10. EBSD IPF map of (a) cross section of the extruded Al6082 wire and (b) longitudinal section of the extruded Al6082 wire – case study S600-18.

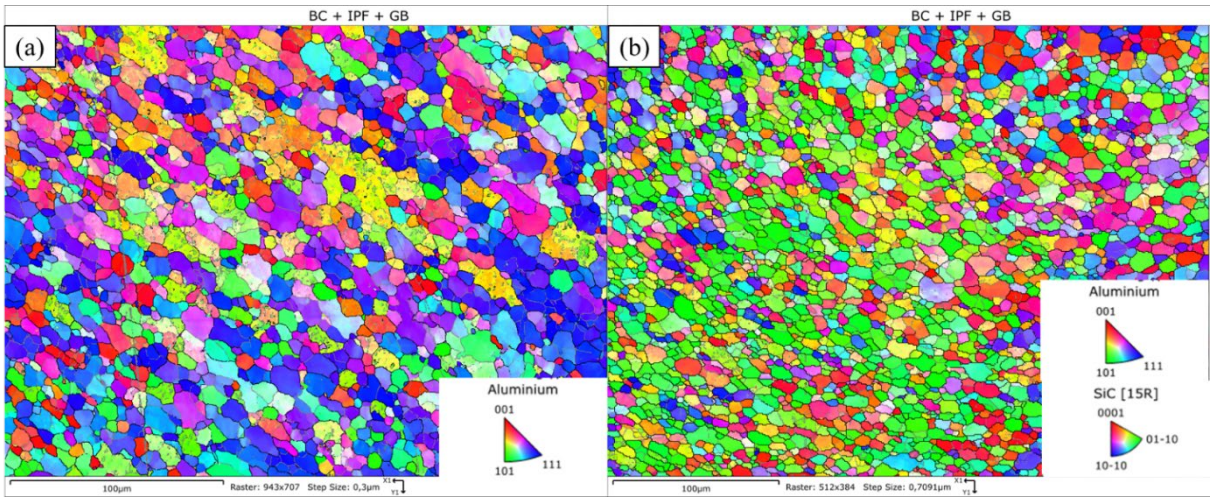

Figure 11. EBSD IPF map of the cross-section of (a) extruded Al 6082 wire (b) Al 6082/SiC composite wire - case study S600-18.

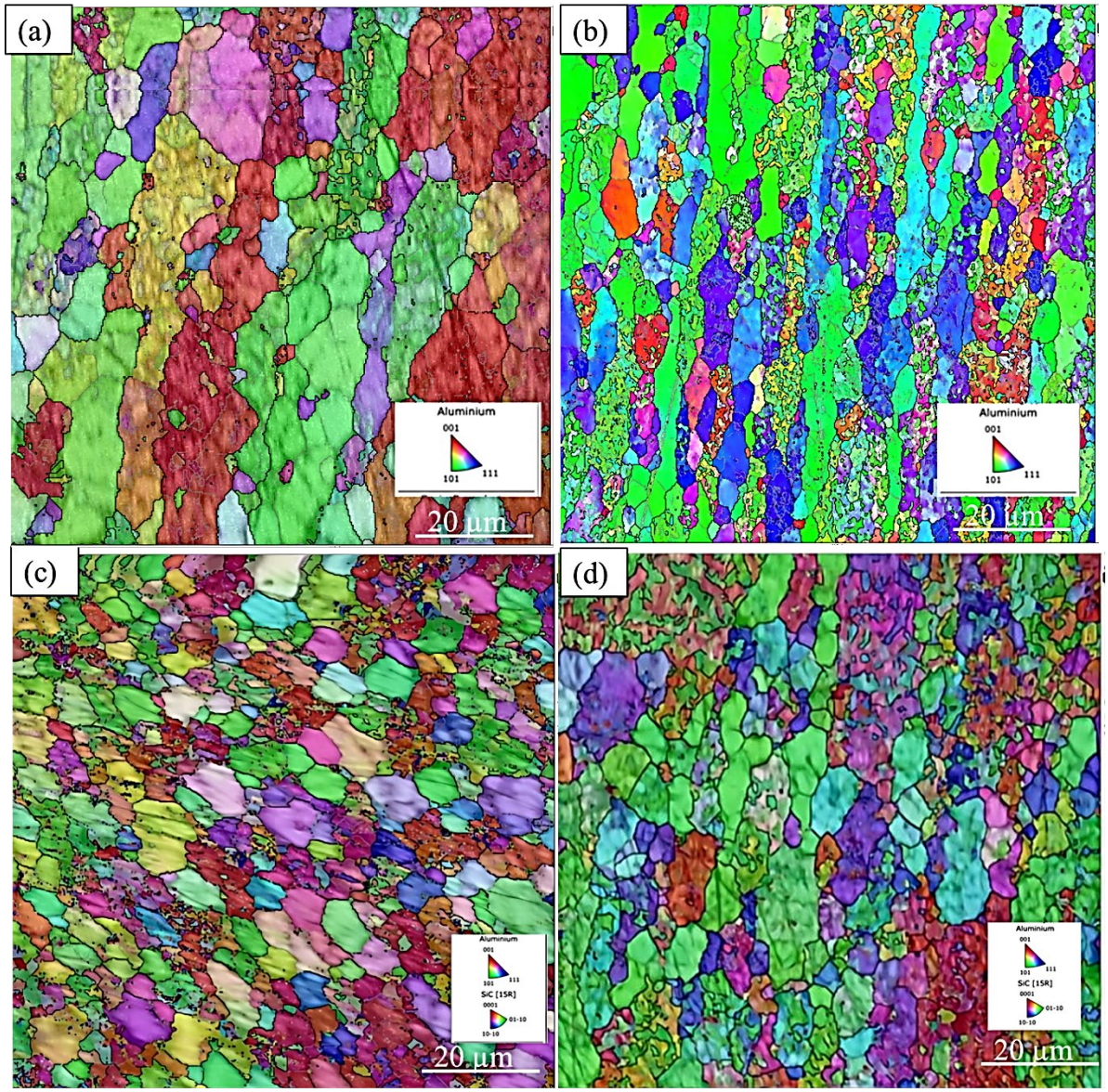

Figure 12. EBSD IPF map of the longitudinal section of sample S600-18 (a) Al 6082 alloy wire at the center (b) Al 6082 alloy wire at the Edges (c) Al 6082/SiC alloy composite wire at the center (d) Al 6082/SiC alloy wire at the Edges – case study S600-18.

The grain boundary maps for extruded Al 6082 wire and Al 6082/SiC wire, corresponding to case study S600-18, are depicted in Fig. 13. Green lines represent low-angle grain boundaries (LAGBs) with misorientation angles between 2° and 10°, while black lines indicate high-angle grain boundaries (HAGBs) with misorientation angles greater than 10°. Boundaries with misorientation angles below 2° are excluded due to the statistical accuracy of EBSD. As illustrated in Fig. 13c, the number of LAGBs, marked by green lines, decreases significantly and is replaced by a considerable number of black lines in the Al 6082/SiC composite wire. In other words, the Al 6082 alloy (Fig. 13a) contains a high number of LAGBs, whereas the Al 6082/SiC alloy has fewer LAGBs. Hence, the fraction of HAGBs, which is 61.8% in the Al 6082 alloy wire, dramatically increases to 74.9% in the Al 6082/SiC composite wire, indicating that LAGBs evolve into HAGBs in Al 6082/SiC composite wire. This is mainly attributed to the addition of SiC for grain refinement and to uniform distribution equiaxed grains which causes continuous dynamic recrystallization (CDRX) as strain-imposed increases during the FSE process of the Al 6082/SiC composite wire. From Fig.13b and Fig.13d, it can be seen that most of the grains are in the range of 0-10 μm diameter. Only a small portion of grains is in the range of 10-12 μm diameter.

In aluminum alloys, basal slip exhibits the lowest critical resolved shear stress, causing the grain lattice to rotate in a direction that favors basal slip during deformation, ultimately leading to texture formation. During extrusion, the metal predominantly flows along the extrusion direction, aligning the deformed grain base plane approximately parallel to this direction. Recrystallized grains typically possess random orientations, allowing fine grains to deform cooperatively by sliding across grain boundaries. This coordinated deformation makes recrystallized grains less likely to develop a strong texture. As the fraction of recrystallized grains increases, they progressively replace deformed grains, resulting in a weakening of the texture. Fig. 14a represents the pole figure for texture analysis of aluminum alloy while Fig.14b and Fig.14c represent the pole figure of aluminum and SiC in Al 6082/SiC composite alloy. The maximum intensity of texture decreases from 10.93 to 3.41 from Al to Al 6082/SiC extruded wire, indicating that the texture tends to be weakened with the addition of SiC. The modification of texture components during FSE processing of Al 6082/SiC wire can be attributed to the accumulation of shear strain. It was reported that texture development in the alloy was related to shear deformation and DRX, because grain and sub-grain boundary migration plays a significant role in the evolution of the texture [34].

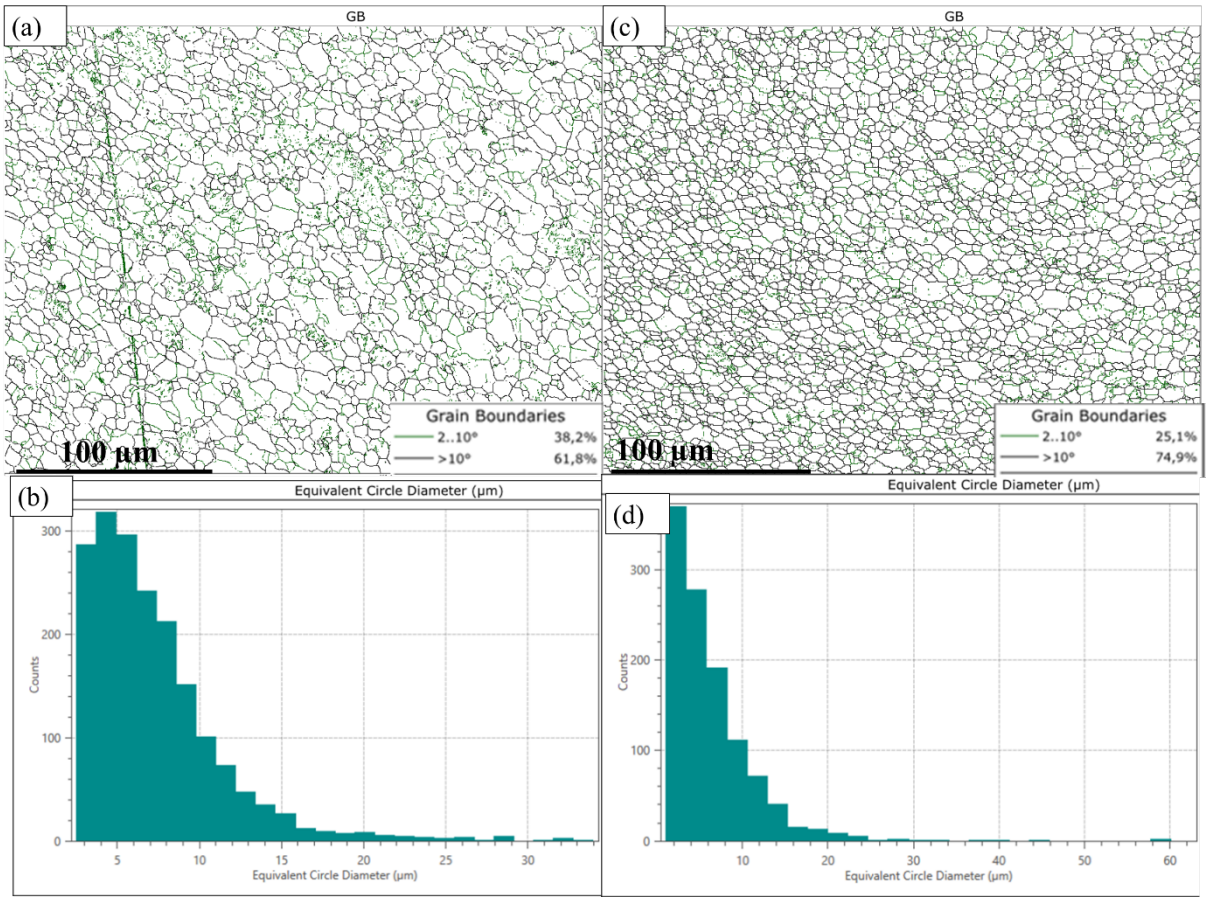

Figure 13. EBSD Grain boundary maps of (a-b) cross section of Al 6082 alloy wire and their corresponding grain distribution, (c-d) cross section of Al 6082/SiC alloy composite wire and their corresponding grain distribution – S600-18 case study.

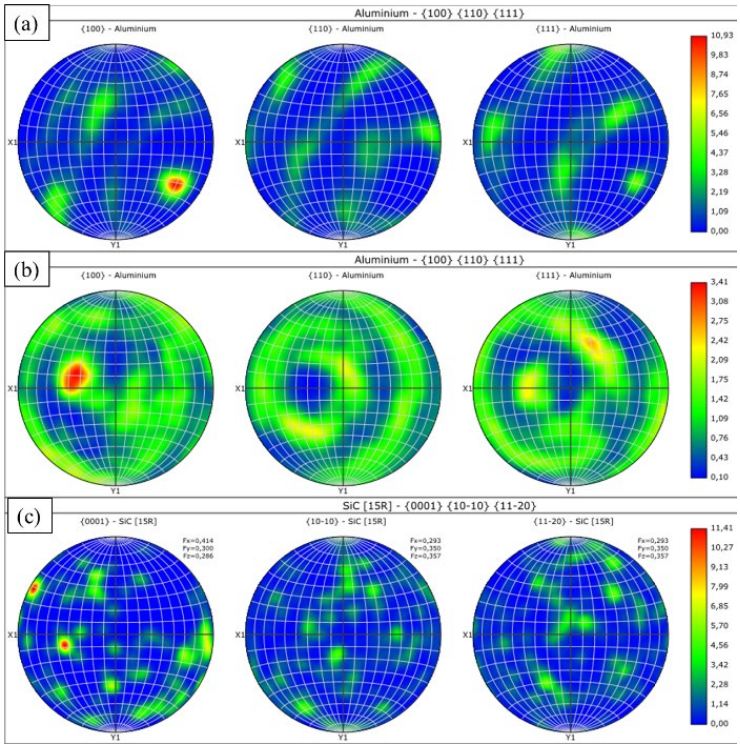

Figure 14. EBSD pole figure of (a) Al in Al 6082 alloy extruded wire (a) Al in Al 6082/SiC composite extruded wire (c) SiC in Al 6082/SiC composite extruded wire.

3.3. Porosity

Porosity measurements were conducted on both reinforced and unreinforced Al 6082 wires (Fig. 15). Significant variations in porosity were observed concerning process parameters. At a low rotational speed of 400 rpm and a low force of 15 kN, the porosity of the extruded wire is notably high. This occurrence can be attributed to the high flow stress exhibited by the material at low temperatures during the FSE process, leading to inadequate bonding between the chips. Increasing the rotational speed from 400 to 600 rpm resulted in a reduction in porosity due to the elevation in temperature, consequently softening the material and enhancing bonding. Furthermore, the porosity of the extruded wire decreases with an increase in extrusion force from 15 to 21 kN. This observation can explain the different behavior between microhardness and UTS previously observed. With constant tool rotation of 400 rpm, increasing UTS and almost constant HV were observed with increasing tool force. For similar average hardness in the three main zones of the wire cross section, i.e. edge, middle radius, and center, the higher porosity observed with lower tool force resulted in poorer mechanical strength. Additionally, it was observed that, with lower extrusion forces, the extrusion rate is reduced, as it will be better discussed in the power consumption paragraph 3.5, allowing sufficient time for grain growth at elevated temperatures. Conversely, increasing the extrusion force enhances the extrusion rate, aligning the process towards traditional extrusion conditions, thereby increasing density and reducing porosity. However, excessive force leads to a disproportionate increase in extrusion rate and a decrease in inlet temperature, resulting in an inability to attain suitable temperatures for dynamic recrystallization, consequently increasing grain size and porosity.

Incorporating SiC as reinforcement within the matrix at low rotational speed poses a challenge, with particle breakage being more probable, leading to significant porosity. Nevertheless, increasing the rotational speed from 400 to 600 rpm for Al 6082/SiC composite wire reduces porosity. This can be attributed to the temperature increase, softening the material, and facilitating the movement of the SiC particles along the extrusion direction.

Similar observations can be made regarding the extrusion force, for which an increase from 15 kN to 21 kN resulted in decreased porosity. The minimum porosity was observed in sample S600-18 for both with and without added reinforcing particles case studies. Notably, rotational speed exhibited a greater effect on porosity. Decreased flow stress and matrix softening at high temperatures facilitate easier rotation and reduced particle breakage, allowing for improved material flow into scattered pores within the base material and smaller pores around the particles, thereby reducing composite porosity. From Fig. 15, it is noteworthy that, at lower processing parameters, the porosity of Al 6082/SiC composite wire is significantly higher compared to unreinforced Al 6082 wires. As processing parameters are increased, this trend reverses. This difference arises because insufficient heat at lower processing parameters leads to incomplete consolidation between chips and the reinforced particles, along with agglomeration of SiC particles at lower rotational speeds (as shown in Fig. 8), which increases porosity. In contrast, unreinforced Al 6082 wires require less heat for extrusion, and their absence of reinforced particles prevents agglomeration, resulting in lower porosity. At higher processing parameters, the dispersion of SiC particles becomes more uniform (see again Fig.

9) and sufficient heat ensures that pores are filled with reinforced particles. Consequently, lower porosity is observed in Al 6082/SiC wires compared to unreinforced wires. It is observed that at 21 kN, the porosity of all three samples is higher compared to sample S600-18. This can be attributed to the contrasting effects of high force on the temperature and material flow already highlighted for the UTS results. Although the overall porosity at 21 kN is lower than that observed at 15 kN, for sample S600-18 the best compromise between extrusion rate and proper material flow is reached. This observation underscores the critical role of processing parameters in determining porosity levels in Al-SiC composite wires during friction stir extrusion, highlighting the importance of optimizing these parameters for achieving desired material properties.

Fig. 16 shows a comparison between Al 6082/SiC composite wire and extruded aluminum wire for the case study S600-18. The lower porosity (read areas in the figure) in Al 6082/SiC composite wire under identical process parameters is clearly visible. This reduction can be attributed to the deformation of metal-based composites, where the presence of a hard reinforcing phase in the soft matrix induces a significant accumulation of local triaxial stress around the particles. As previously mentioned, increased process temperature facilitates dislocation release, reducing local stress around the particles.

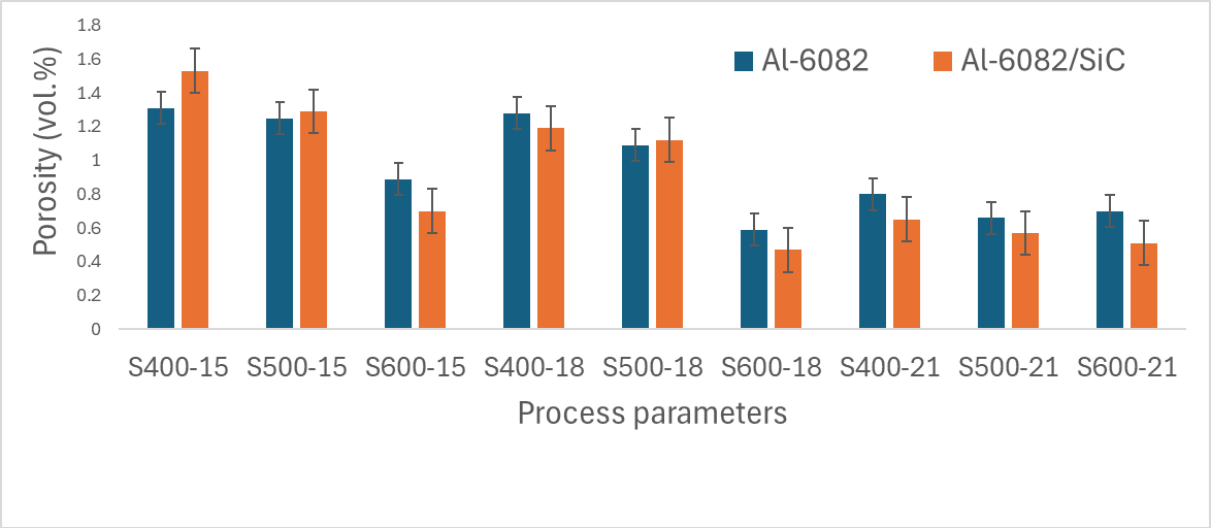

Figure 15. volumetric porosity measurement in Al 6082 wire and Al 6082/SiC Extruded wire.

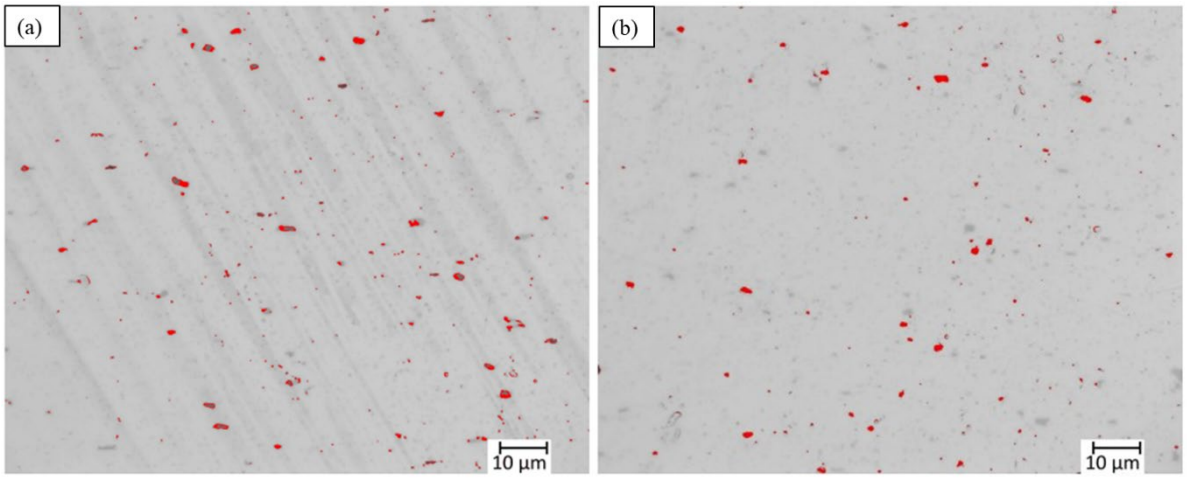

Figure 16. OM images of the cross-section of the produced sample at S600-18 (a) Al 6082 alloy wire (b) Al6082/SiC composite wire.

3.4. Testing surface roughness

Surface roughness is a crucial factor in the quality of wires. To investigate the effect of process parameters and reinforcement particles on the surface roughness of the extruded wires, a surface roughness tester and the Profilm Online commercial software were used. In this study, arithmetic mean height (Ra) was considered to characterize the surface roughness of samples. It has been observed that tool rotation and tool force have a significant influence on the surface roughness of the wires. At low RPM and low force, the heat input is low, resulting in cold tearing and brittleness, and the surface roughness is significantly high. By increasing the rotational speed and tool force, smoother wire surfaces have been observed. The minimum Ra, corresponding to a smoother surface finishing, is obtained for the S600-18 case study. It is worth mentioning that a further increase of heat input, i.e. increase of tool rotation and/or force, results in increased surface roughness. This is due to the high-temperature hot cracks in the wire, as already observed in paragraph 3.1. Fig. 17 illustrates the 3D roughness profile of Al 6082 wire and Al 6082/SiC wire for the case studies S600-18 and S400-15. As the case study S600-18 is considered, surface roughness (Ra) of 2.09 was measured for the Al 6082 wire (Fig. 17b), which was significantly lower as compared to the one of the composite wire, equal to 3.89 (Fig. 17a). This increased roughness is attributed to the presence of abrasive SiC particles in the aluminum matrix. The addition of SiC generates more heat and allows SiC to penetrate deeper into the subsurface, producing more plasticized material and causing the dislodging of SiC particles from the aluminum matrix. Inadequate flushing of the plasticized material leads to the formation of a thicker recast layer. For the case study S400-15, the same trend was observed although higher values have been measured for both the Al 6082 wire (Ra = 3.03) and the Al 6082/SiC wire (Ra = 4.52). The latter is characterized by higher peak-to-valley heights, deeper cavities, and more surface irregularities. This increase in surface roughness with decreasing heat input can be attributed to the insufficient bonding between chips, as well as to the presence of micro voids and cracks. (The macroscopic appearance of the extruded wires roughness at lower process parameters can be seen in Figure 3).

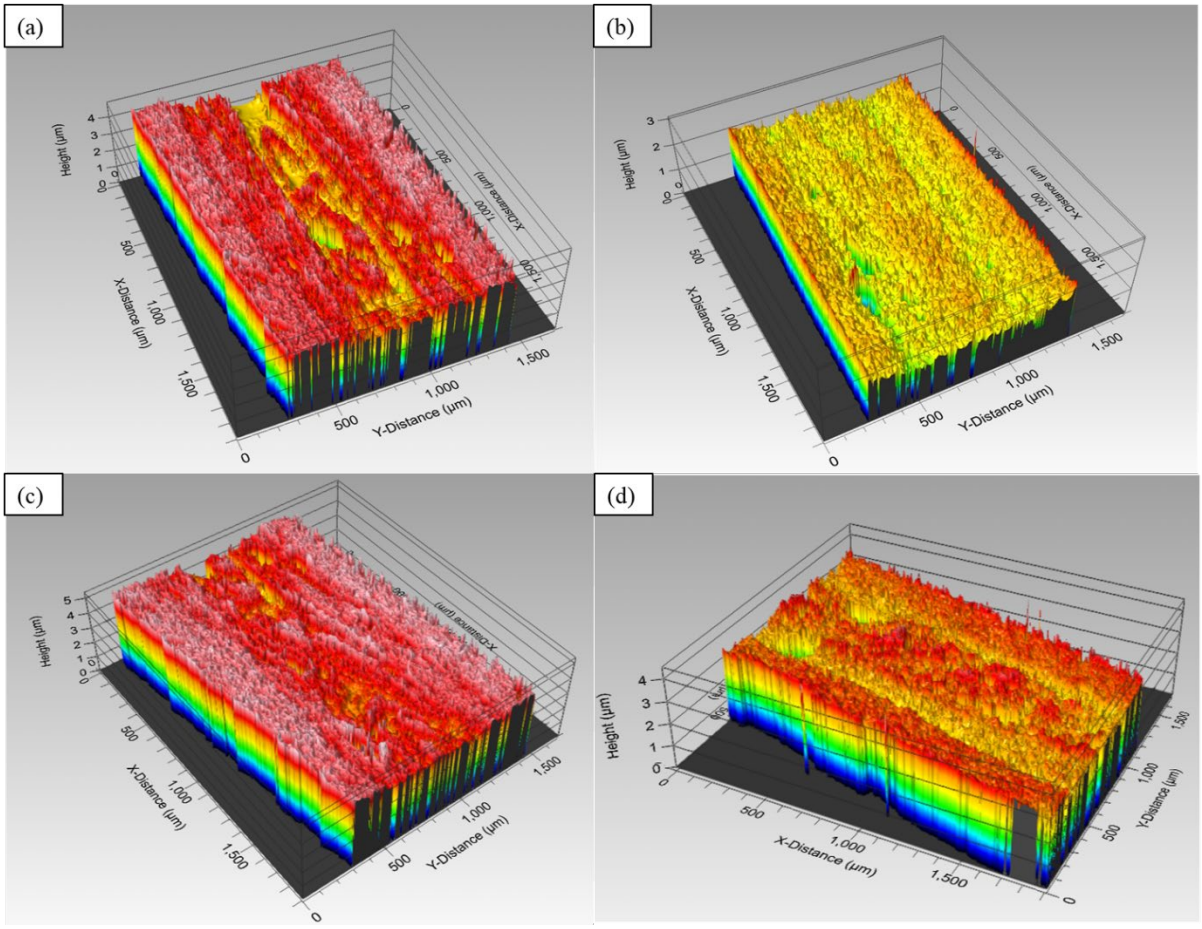

Figure 17. 3D Surface roughness profile of (a) Al6082/SiC composite wire for sample S600-18 (b) Al 6082 alloy wire for sample S600-18 (c) Al6082/SiC composite wire for sample S400-15 (d) Al 6082 alloy wire for sample S400-15.

3.5. Power consumption

Previous research [31] has delved into analyzing the power absorbed by machinery during the various process phases, aiming to delineate the contribution of each phase. In contrast, this study scrutinizes the power utilization under different process parameters to ascertain its impact on power consumption in the production of both Al 6082/SiC composite wire and unreinforced aluminum wire. It was noted that power consumption remained consistent, irrespective of the presence of reinforcement particles. Fig. 18(a) illustrates power consumption across different tool rotational speeds while maintaining a constant force of 21kN, with rotational speeds of 400, 500, and 600 rpm being examined. The results reveal a uniform power consumption trend alongside an increase in processing time as rpm decreases. This phenomenon can be attributed to lower heat generation at lower rpm, resulting in a diminished extrusion rate and subsequently prolonged processing times. Notably, the maximum power efficiency was observed at 600 rpm under constant force. Conversely, Fig. 18b depicts power consumption variation under constant rotational speed (600 rpm) with varying forces of 15, 18, and 21kN. Analysis of the graph indicates a direct correlation between force increment and power consumption increase. Higher forces correspond to heightened extrusion rates, thereby reducing processing time. Based on the observation, the minimum power consumption outcomes were achieved at 600 rpm and

15kN force. It is worth noting that, although the minimum power consumption was measured for the S600-15 case study, the S600-18 case study, which corresponds to the best mechanical and microstructural properties among the ranges investigated, showed only a minimal increase in power absorption and lower duration, resulting in lower energy required.

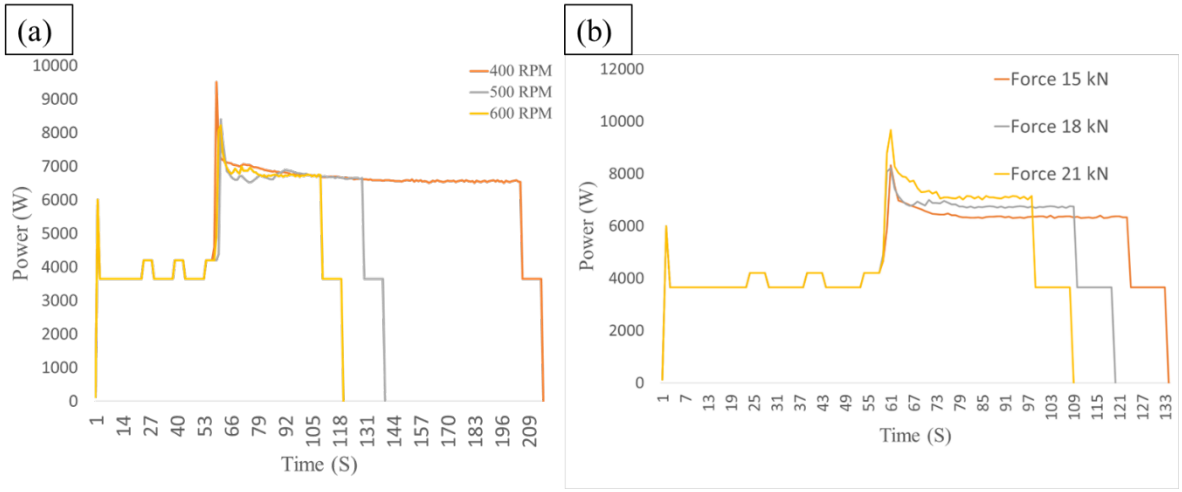

Figure 18. power consumption as a function of (a) tool rotation (constant force equal to 21 kN) and (b) force (constant tool rotation equal to 600 rpm).

Finally, to assess the viability of using extruded wire as a filler rod in the Wire Arc Additive Manufacturing (WAAM) process, both the Al6082/SiC wire and the Al6082 alloy wire obtained with tool rotation of 600rpm and tool force of 18kN, were successfully deposited by wire-arc welding. Fig. 19 illustrates the deposition of the extruded Al6082/SiC wire in the WAAM process. The experiments utilized a substrate plate made of Al 6062 measuring 100 mm × 50 mm × 5 mm.

Figure 19. extruded wire deposition in the WAAM process.

Summary and Conclusion

In this research, Al 6082/SiC composites wire and Al 6082 wire were fabricated from chips through the FSE technique under different process parameters. The effects of process parameters and SiC reinforcement on the microstructure and mechanical behavior of the extruded wires were investigated via SEM, EDS, EBSD, Vicker hardness, bending, and tensile test. Based on the obtained results, the following main conclusions can be drawn:

- Defect-free bonding between reinforcement and aluminum matrix can be established when uniform and homogeneous dispersion of the SiC particles is achieved. Among the

parameters investigated, optimal conditions have been found with tool rotation of 600 rpm and tool force of 18 kN.

- The use of SiC reinforcement results in an increase in the mechanical properties of the wires, with maximum microhardness of 106.8 HV, which is 12.5% higher than unreinforced Al 6082 wire, and maximum tensile strength of 216 MPa, which is 12.78% higher than unreinforced Al 6082 wire, obtained for the S600-18 case study.
- Low heat input results in the presence of SiC agglomerates, reducing the mechanical properties of the wires.
- The chips undergo solid bonding and continuous dynamic recrystallization during the process. However, the average grain size is smaller close to the edge of the wire than in the center due to the increased shear strain close to the tool edge and extrusion matrix. The average grain size in the Al 6082/SiC composite decreases, with respect to the unreinforced wire, to 5.6 μm. Additionally, the proportion of LAGBs in the Al-SiC composite decreased to 25.1%, suggesting that the incorporation of SiC can promote the occurrence of dynamic recrystallization and weak texture.
- In the Al 6082/SiC wires produced at S600-18, the better distribution of reinforcing particles and a stronger bond between SiC particles and the aluminum matrix led to lower porosity with respect to both wires produced under "colder" process conditions and the wire produced with the same process parameters and no SiC reinforcement (P = 0.47%). When poor process parameters are selected, the porosity of the reinforced wires is lower than the one of the unreinforced wires due to the presence of SiC particle agglomeration.
- The Power consumption decreases with increasing tool rotation and tool force. Considering the most efficient process conditions, significant savings can be obtained with respect to conventional production routes. Additionally, process time, i.e. extrusion rate, decreases with increasing tool rotation and toll force leading to lower energy requirement for the process.

Future work will include the analysis of the WAAM welds obtained with the recycled wires in order to identify the best FSE process conditions for this application.

Acknowledgments

This study was carried out within the research activities of project "PERPETUAL 100% Material utilization using sOlid sTate recycling and Additive Manufacturing for production and repairing of aluminum components – PERPETUAL MOTION" (2022X5RPSM PRIN 2022), financed by the by the European Community – Next Generation EU. This manuscript reflects only the Authors' views and opinions, neither the European Union nor the European Commission can be considered responsible for them.

References

[1] N. Gangil, A.N. Siddiquee, S. Maheshwari, Aluminium based in-situ composite fabrication through friction stir processing: A review, J Alloys Compd 715 (2017) 91–104. https://doi.org/10.1016/j.jallcom.2017.04.309.

[2] J. Cui, H.J. Roven, Recycling of automotive aluminum, Transactions of Nonferrous Metals Society of China (English Edition) 20 (2010) 2057–2063. https://doi.org/10.1016/S1003-6326(09)60417-9.

[3] Y. Zhang, M. Sun, J. Hong, X. Han, J. He, W. Shi, X. Li, Environmental footprint of aluminum production in China, J Clean Prod 133 (2016) 1242–1251. https://doi.org/10.1016/j.jclepro.2016.04.137.

[4] P.K. Krishnan, J.V. Christy, R. Arunachalam, A.H.I. Mourad, R. Muraliraja, M. Al-Maharbi, V. Murali, M.M. Chandra, Production of aluminum alloy-based metal matrix composites using scrap aluminum alloy and waste materials: Influence on microstructure and mechanical properties, J Alloys Compd 784 (2019) 1047–1061. https://doi.org/10.1016/j.jallcom.2019.01.115.

[5] S. Al-Alimi, S. Shamsudin, N.K. Yusuf, M.A. Lajis, W. Zhou, D.H. Didane, S. Sadeq, Y. Saif, A. Wahib, Z. Harun, Recycling Aluminium AA6061 Chips with Reinforced Boron Carbide (B4C) and Zirconia (ZrO2) Particles via Hot Extrusion, Metals (Basel) 12 (2022). https://doi.org/10.3390/met12081329.

[6] A.E. Tekkaya, M. Schikorra, D. Becker, D. Biermann, N. Hammer, K. Pantke, Hot profile extrusion of AA-6060 aluminum chips, J Mater Process Technol 209 (2009) 3343–3350. https://doi.org/10.1016/j.jmatprotec.2008.07.047.

[7] B. Wan, W. Chen, T. Lu, F. Liu, Z. Jiang, M. Mao, Review of solid state recycling of aluminum chips, Resour Conserv Recycl 125 (2017) 37–47. https://doi.org/10.1016/j.resconrec.2017.06.004.

[8] Y. Chen, H. Liu, Y. Wu, K. Yan, J. Ju, H. Teng, D. Song, J. Jiang, J. Bai, Comparative study of the microstructure evolution and mechanical properties of Zn-0.1Mg-0.02Ca alloy under cold rolling and ECAP, Materials Science and Engineering: A 908 (2024). https://doi.org/10.1016/j.msea.2024.146765.

[9] S. Whalen, N. Overman, V. Joshi, T. Varga, D. Graff, C. Lavender, Magnesium alloy ZK60 tubing made by Shear Assisted Processing and Extrusion (ShAPE), Materials Science and Engineering: A 755 (2019) 278–288. https://doi.org/10.1016/j.msea.2019.04.013.

[10] K. Suzuki, X.S. Huang, A. Watazu, I. Shigematsu, N. Saito, Recycling of 6061 Aluminum Alloy Cutting Chips Using Hot Extrusion and Hot Rolling, Materials Science Forum 544–545 (2007) 443–446. https://doi.org/10.4028/www.scientific.net/msf.544-545.443.

[11] G. Buffa, D. Baffari, G. Ingarao, L. Fratini, Uncovering Technological and Environmental Potentials of Aluminum Alloy Scraps Recycling Through Friction Stir Consolidation, International Journal of Precision Engineering and Manufacturing - Green Technology 7 (2020) 955–964. https://doi.org/10.1007/s40684-019-00159-5.

[12] K. Kondoh, T. Luangvaranunt, T. Aizawa, 322 to 325 Special Issue on Environmentally Benign Manufacturing and Material Processing Toward Dematerialization, 2002.

[13] D. Paraskevas, K. Vanmeensel, J. Vleugels, W. Dewulf, Y. Deng, J.R. Duflou, Spark plasma sintering as a solid-state recycling technique: The case of aluminum alloy scrap consolidation, Materials 7 (2014) 5664–5687. https://doi.org/10.3390/ma7085664.

[14] B.P. Sahoo, & D. Das, Investigation on Reinforcement Incorporation Factor and Microstructure of Al 7075/Submicron-TiB 2 Metal Matrix Composites Processed through a Modified Liquid Metallurgy Technique, (n.d.). https://doi.org/10.1007/s40799-020-00429-x/Published.

[15] N.K. Bhoi, H. Singh, S. Pratap, Developments in the aluminum metal matrix composites reinforced by micro/nano particles – A review, J Compos Mater 54 (2020) 813–833. https://doi.org/10.1177/0021998319865307.

[16] N. Ahamad, A. Mohammad, M.L. Rinawa, K.K. Sadasivuni, P. Gupta, Correlation of structural and mechanical properties for Al-Al2O3-SiC hybrid metal matrix composites, J Compos Mater 55 (2021) 3267–3280. https://doi.org/10.1177/00219983211011537.

[17] S. Slathia, M.I. Ul Haq, A. Raina, Fabrication and mechanical characterization of AA2024 - ZrO2 - Gr hybrid composite, in: AIP Conf Proc, American Institute of Physics Inc., 2018. https://doi.org/10.1063/1.5051303.

[18] J.B. Fogagnolo, E.M. Ruiz-Navas, M.A. Simón, M.A. Martinez, Recycling of aluminium alloy and aluminium matrix composite chips by pressing and hot extrusion, in: J Mater Process Technol, 2003: pp. 792–795. https://doi.org/10.1016/S0924-0136(03)00380-7.

[19] B.P. Sahoo, D. Das, A.K. Chaubey, Strengthening mechanisms and modelling of mechanical properties of submicron-TiB2 particulate reinforced Al 7075 metal matrix composites, Materials Science and Engineering: A 825 (2021). https://doi.org/10.1016/j.msea.2021.141873.

[20] N.R.J. Hynes, D.S.S.P. Kumar, M.V. Prabhu, M.A. Ali, M.H. Raza, C.I. Pruncu, Investigating the parametric effects on wire electric discharge machining performance in processing AA1050-5 wt.% SiC composite with zinc-coated brass wire, Journal of the Brazilian Society of Mechanical Sciences and Engineering 44 (2022). https://doi.org/10.1007/s40430-022-03427-9.

[21] B. Xiong, Z. Xu, Q. Yan, C. Cai, Y. Zheng, B. Lu, Fabrication of SiC nanoparticulates reinforced Al matrix composites by combining pressureless infiltration with ball-milling and cold-pressing technology, J Alloys Compd 497 (2010). https://doi.org/10.1016/j.jallcom.2010.02.184.

[22] L. Zhang, H. Xu, Z. Wang, Q. Li, J. Wu, Mechanical properties and corrosion behavior of Al/SiC composites, J Alloys Compd 678 (2016) 23–30. https://doi.org/10.1016/j.jallcom.2016.03.180.

[23] E. Mohammad Sharifi, F. Karimzadeh, M.H. Enayati, Fabrication and evaluation of mechanical and tribological properties of boron carbide reinforced aluminum matrix nanocomposites, Mater Des 32 (2011) 3263–3271. https://doi.org/10.1016/j.matdes.2011.02.033.

[24] J.Z. Gronostajski, H. Marciniak, A. Matuszak, Production of composites on the base of AICu4 alloy chips, 1996.

[25] J.B. Fogagnolo, E.M. Ruiz-Navas, M.A. Simón, M.A. Martinez, Recycling of aluminium alloy and aluminium matrix composite chips by pressing and hot extrusion, in: J Mater Process Technol, 2003: pp. 792–795. https://doi.org/10.1016/S0924-0136(03)00380-7.

[26] M. Samuel, Reinforcement of recycled aluminum-alloy scrap with Saffil ceramic fibers, J Mater Process Technol 142 (2003) 295–306. https://doi.org/10.1016/S0924-0136(03)00585-5.

[27] A.M. Razzaq, D.L. Majid, M.R. Ishak, U.M. Basheer, Effect of fly ash addition on the physical and mechanical properties of AA6063 alloy reinforcement, Metals (Basel) 7 (2017). https://doi.org/10.3390/met7110477.

[28] D. Baffari, G. Buffa, D. Campanella, L. Fratini, Al-SiC Metal Matrix Composite production through Friction Stir Extrusion of aluminum chips, in: Procedia Eng, Elsevier Ltd, 2017: pp. 419–424. https://doi.org/10.1016/j.proeng.2017.10.798.

[29] X. Li, H. Das, M. Pole, L. Li, A. Soulami, G.J. Grant, D.R. Herling, M. Efe, Exceptional strength and wear resistance in an AA7075/TiB2 composite fabricated via friction consolidation, Mater Des 242 (2024) 113006. https://doi.org/10.1016/j.matdes.2024.113006.

[30] Z. Sherafat, M.H. Paydar, R. Ebrahimi, Fabrication of Al7075/Al, two phase material, by recycling Al7075 alloy chips using powder metallurgy route, J Alloys Compd 487 (2009) 395–399. https://doi.org/10.1016/j.jallcom.2009.07.146.

[31] G. Buffa, D. Campanella, M. Adnan, U. La Commare, G. Ingarao, L. Fratini, Improving the Industrial Efficiency of Recycling Aluminum Alloy Chips Using Friction Stir Extrusion: Thin Wires Production Process, International Journal of Precision Engineering and Manufacturing - Green Technology (2024). https://doi.org/10.1007/s40684-023-00573-w.

[32] S. Ngernbamrung, Y. Suzuki, N. Takatsuji, K. Dohda, Investigation of surface cracking of hot-extruded AA7075 billet, in: Procedia Manuf, Elsevier B.V., 2018: pp. 217–224. https://doi.org/10.1016/j.promfg.2018.07.212.

[33] B. Song, S. Dong, C. Coddet, Rapid in situ fabrication of Fe/SiC bulk nanocomposites by selective laser melting directly from a mixed powder of microsized Fe and SiC, Scr Mater 75 (2014) 90–93. https://doi.org/10.1016/j.scriptamat.2013.11.031.

[34] G. Girish, V. Anandakrishnan, Investigations on microstructural and texture evolution during recursive friction stir processing of aluminium 7075 alloy, Mater Res Express 6 (2019) 126574. https://doi.org/10.1088/2053-1591/ab58ed.